Available online at www.sciencedirect.com
SCIENCE DIRECT®
Journal of Power Sources 141 (2005) 307–315
JOURNAL OF POWER SOURCES
www.elsevier.com/locate/jpowsour

Simulation of passive thermal management system for lithium-ion battery packs

Andrew Mills, Said Al-Hallaj*

Department of Chemical and Environmental Engineering, Center for Electrochemical Science and Engineering, Illinois Institute of Technology, 10 West 33rd St., Chicago, IL 60616, USA

Received 14 September 2004; accepted 30 September 2004
Available online 7 December 2004

Abstract

A passive thermal management system that uses a phase change material (PCM) is designed and simulated for a lithium-ion (Li-ion) laptop battery pack. The problem of low thermal conductivity of the PCM was significantly improved by impregnating an expanded graphite (EG) matrix with the PCM. The heat generation rate for a commercial 186502.2 Ah Li-ion battery was experimentally measured for various constant power discharges. Simulation of the battery pack, composed of six Li-ion batteries, shows that safe operation of the battery pack during the most extreme case requires the volume of the battery pack be almost doubled to fit sufficient PCM in the pack. Improving the properties of the PCM composite have the potential to significantly reduce the volume increase in comparison to the original battery pack volume.

Keywords: Li-ion battery; Laptop battery packs; Thermal management; PCM; Thermal performance

1. Introduction

Lithium-ion (Li-ion) batteries provide an attractive alternative to other battery chemistries in part due to high-energy storage density and competitive cost. However, Li-ion batteries generate significant heat during high power discharge, in some cases shortening the battery life or posing a safety hazard. Advances in laptop computer technology require increasing electric power and decreasing density. Li-ion batteries provide high energy density at low cost, but are limited in application because of the high heat generation rates coupled with the adverse effect of temperature on battery life [1]. Laptop battery packs require multiple Li-ion cells to be stored close together and provide high electric power, which can lead to temperatures that degrade the battery life [2]. Traditional cooling systems, such as an air-cooling system with an electric fan, are not attractive solutions due to the bulkiness and additional power requirements. Previous research with Li-ion battery packs has demonstrated that a passive thermal management system using a phase change material (PCM) is a viable solution [3].

The passive thermal management system utilizes the latent heat stored in a material as it changes phase over a small temperature range. PCMs have been used in numerous applications ranging from building materials to solar energy systems. Challenges associated with applying PCMs have been addressed in the corresponding research [4]. PCMs typically have low thermal conductivity, typically limiting the applications of PCM to environments with a low heat transfer rate. However, in this work we utilize an expanded graphite (EG) matrix impregnated with the PCM to increase the overall thermal conductivity.

2. Design procedure

The two most important considerations for the design of a passive thermal management system for lithium-ion battery

* Corresponding author. Tel.: +1 312 567 5118; fax: +1 312 567 6914.
E-mail address: alhallaj@iit.edu (S. Al-Hallaj).

0378-7753/$ – see front matter © 2004 Elsevier B.V. All rights reserved.
doi:10.1016/j.jpowsour.2004.09.025

Nomenclature

A	heat transfer area
C	discharge rate for constant current discharge (C/1 rate for 2.2 Ah battery is 2.2 A)
C_p	specific heat capacity
I	current
k	thermal conductivity
m	mass
n	number of trials
P	analogous discharge rate for constant power discharge (P/1 rate for 8.25 Wh is 8.25 W)
$\dot{q}$	heat generation rate
s	standard error in measuring the mean
t	time
T	temperature
U	overall heat transfer coefficient
V	voltage
V	volume
x	position along horizontal axis
y	position along vertical axis

Subscripts

avail	volume available between batteries and battery pack
comp	volume of PCM/EG composite
conv	heat transferred through convection
elect	heat generation rate of pack electronics
gen	heat generation rate for battery
ocv	open circuit voltage
op	operating voltage of battery under load
stor	heat storage
total	total heat generation rate

Greek letters

ρ	density
σ	standard deviation

packs are the heat generation characteristics of the batteries and the thermal storage characteristics of the PCM.

2.1. Heat generation

The battery heat generation depends on the discharge profile, as shown in Eq. (1). In this study, we assume that the batteries will provide a constant power level during the discharge. The heat generated by the battery during a constant power discharge was measured experimentally, as will be described later in this work:

$$\dot{q}_{\text{gen}} = I(V_{\text{ocv}} - V_{\text{op}}) - IT\frac{\mathrm{d}V_{\text{ocv}}}{\mathrm{d}T} \quad (1)$$

$I > 0$ for discharge.

2.2. PCM characteristics

The role of PCM in the thermal management system is to absorb and store the heat generated by the batteries while minimizing the temperature variation of the battery pack. The latent heat and melting temperature of the PCM govern the amount of heat that can be stored and the temperature at which this process occurs. Paraffin wax (Rubitherm RT-42), was used as the PCM in this study due to a high specific latent heat, melting temperatures within the operating temperature of the batteries, and low-cost commercial availability.

One significant disadvantage of paraffin wax is its low thermal conductivity, about $0.2\,\mathrm{W\,m^{-1}\,K^{-1}}$, thereby limiting the rate of heat dissipation and absorption. An expanded graphite (EG) matrix with high thermal conductivity was impregnated with paraffin to produce a composite material (PCM/EG) having high thermal conductivity and high specific latent heat.

2.3. PCM/EG composite

The expanded graphite is formed from flake graphite through a heat treatment process that breaks the weak van der Waals bonds between the sheets of carbon that make up the flake graphite. This process greatly increases the porosity of the graphite and similarly decreases the bulk density. Large volumes of expanded graphite particles are then compacted to form a solid matrix of graphite. The degree of compaction dictates the resulting porosity and the thermal conductivity of the matrix in the direction perpendicular to compaction (i.e. more compaction decreases the porosity and increases the thermal conductivity in the perpendicular plane). Fig. 1 shows the change in thermal conductivity of the graphite matrix with the change in density of the matrix measured in earlier work by the current authors [5]. The thermal conductivity is shown for the direction perpendicular to the direction of compaction and parallel to the direction of compaction. The lines in the figure are results from the literature [6–8].

The PCM/EG composite is then formed by submerging the EG matrix in liquid PCM. Capillary forces pull the PCM

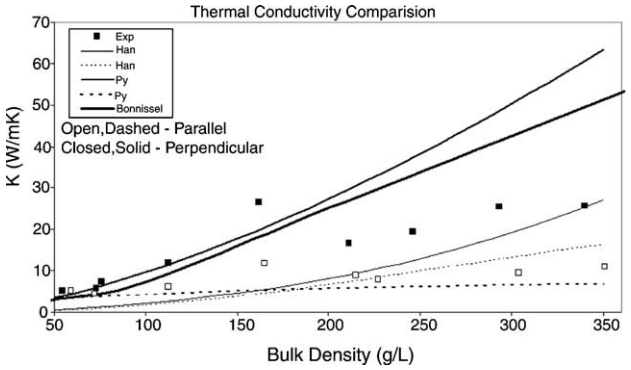

Fig. 1. Thermal conductivity of PCM/EG composite for various graphite matrix densities (ref. [5]).

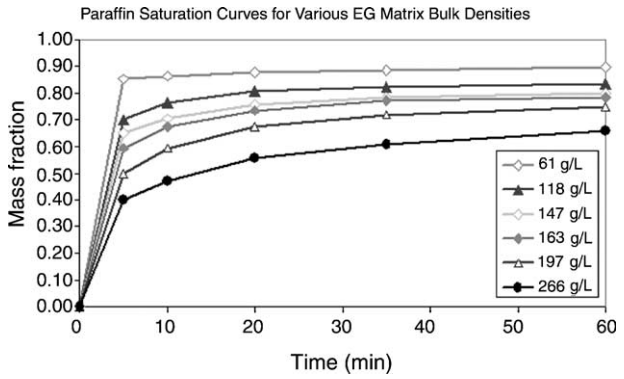

Fig. 2. Change in PCM mass fraction of composite while submerged in liquid PCM (ref. [5]).

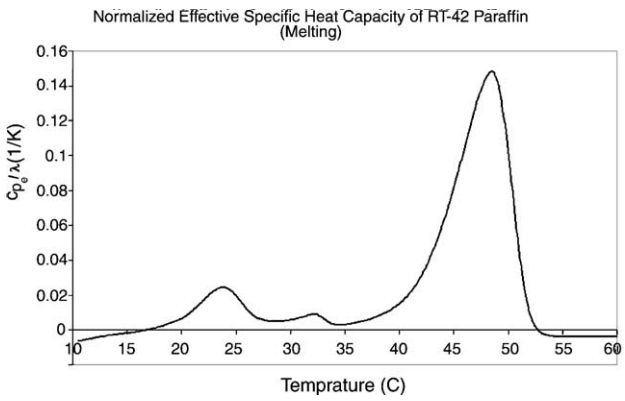

Fig. 3. Normalized DSC curve for RT-42 paraffin (ref. [5]).

into the matrix where it remains after the matrix is removed from the liquid PCM bath. Fig. 2 shows the mass fraction of the PCM in the composite as a function of time submerged in the liquid PCM. Details of the fabrication process and characteristics of the PCM/EG composites are explained elsewhere [5]. The parameters of the composite used in this study are shown in Table 1.

2.4. Modeling phase change process

In many cases, modeling the phase change process of materials that melt over a temperature range can be complicated. However, Farid et al. [9], developed a modeling tool that uses the effective heat capacity of the PCM, where the phase change process is treated as a temperature dependent change in the specific heat of the material [9]. A curve fit to the differential scanning calorimetry (DSC) curve of the paraffin is used to determine the effective heat capacity at various temperatures, as shown in Fig. 3. Details on the experimental method for obtaining this curve for the PCM used in this work can be found elsewhere [5]. The curve is normalized so that the area under the large peak is unity to allow the curve to be scaled to the latent heat of the paraffin.

2.5. Unsteady 2D modeling and simulation of battery pack

Simulations were performed of a battery pack with the passive thermal management system using the finite element software PDEase2D (Macsyma Inc., Massachussets, USA). The simulations solve the 2D unsteady heat conduction equation, Eq. (2). The thermal conductivity of the batteries was taken from ref. [12] while the geometry, density, and heat capacity were all measured for a commercial 2.2 Ah 18650 Li-ion cells (LG Chemicals) used to determine the heat generation rates. Fig. 4 is a schematic of the battery pack.

$$\rho C_p \frac{\partial T}{\partial t} = k\left(\frac{\partial^2 T}{\partial x^2} + \frac{\partial^2 T}{\partial y^2}\right) + \dot{q}_{\text{total}} \quad (2)$$

An electronics pack inside the battery pack was simulated with a total heat generation equal to the sum of the electronic components presented by Maleki and Shamsuri [2], scaled to the power output of the battery pack. The heat was assumed to be uniformly generated throughout a 2-mm thick layer of printed circuit board (PCB) material and placed on a 2-mm thick layer of PCB without heat generation. The properties of PCB can be found in the literature [2].

The boundary conditions for the simulation were natural convection on Side A and the bottom, Side B of the laptop [11]. The heat transfer coefficients between the laptop body and Sides C and D were approximated with very low heat transfer coefficients: $h_C = 1.5\,\text{W m}^{-2}\,\text{K}^{-1}$ and $h_D = 2.25\,\text{W m}^{-2}\,\text{K}^{-1}$. These coefficients were estimated from rough simulations of the battery pack close to a body with dimensions of a typical laptop.

Table 1
Thermo-physical properties of PCM/EG composite used in this study

Property	Value
Thermal conductivity ($\text{W m}^{-1}\,\text{K}^{-1}$)	16.6
Latent heat (J g^{-1})	127
Specific heat ($\text{J g}^{-1}\,\text{K}^{-1}$)	1.98
Bulk density of composite (g m^{-3})	7.89E+05
Bulk density of graphite (g m^{-3})	2.10E+05

3. Experimental results

The heat generation rates during the discharge of the 2.2 Ah 18650 Li-ion battery were measured experimentally. The heat generation is determined from an energy balance, Eq. (3).

$$\dot{q}_{\text{gen}} = \dot{q}_{\text{stor}} + \dot{q}_{\text{conv}}$$

$$\dot{q}_{\text{gen}} = mC_p \frac{\text{d}T}{\text{d}t} + UA\,\Delta T \quad (3)$$

3.1. Experimental setup

The battery was insulated with Styrofoam during the discharge to reduce convection heat transfer. The experimental

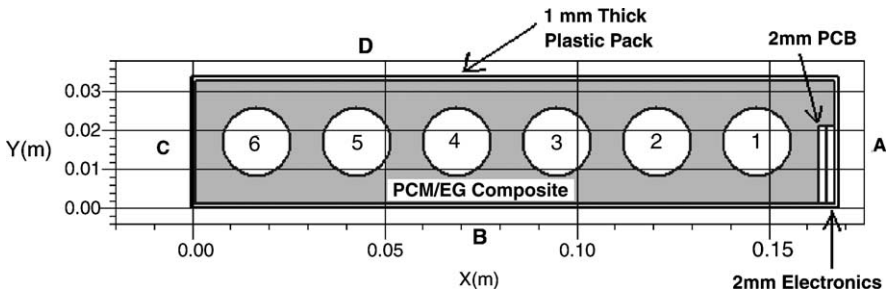

Fig. 4. Schematic of battery pack used in simulations, note that pack geometry changes for different simulations.

setup is shown in Fig. 5. Metal cylinders, 6061-T6 aluminium and copper, with the same dimension as the 18650 Li-ion battery were used to determine the *UA* value of the setup, as described later in the experimental setup.

Two thermocouples (Omega Engineering Inc., T-Type SA1-T) were placed on opposite sides at the middle of the battery. A third thermocouple was placed outside of the insulation, approximately 30 cm from the center of the battery, to measure the ambient air temperature. A thin, high-resistance heating wire (Omega, Nickel–Chromium NI-80) was spirally wound around the battery and cylinders to control the temperature during the calibration tests. The wire was fashioned to the cylinders using thin, vinyl electrical tape.

The battery was discharged and charged using an Arbin Battery Cycler (Model. No. BT2000, College Station, Texas, USA). The cycler was used to record the battery and thermocouple data every minute. Prior to the heat generation tests the open circuit voltage (OCV) of the Li-ion cell was estimated by discharging the cell at a very low rate, *C*/24.

3.2. Calibration

The *UA* value of the cylinders within the insulation was determined experimentally by heating metal cylinders to a high temperature then recording the temperature from each thermocouple as the cylinders cooled. Solving Eq. (3) for the case of $\dot{q}_{\text{gen}} = 0$, with $Bi \ll 0.1$, leads to the following relationship, Eq. (4). The ambient temperature is taken as the mean of the temperature during the cooling cycle. The temperature of the cylinder or battery is found from the mean of thermocouples 1 and 2.

$$\frac{\ln(\Delta T)}{t} = -\frac{UA}{mC_p} \tag{4}$$

The cylinders were slowly heated to 60 °C by passing current through the heating wire. Once the temperature exceeded 60 °C, the current was stopped and the cylinder was allowed to cool. The temperatures were recorded until the temperature of the cylinder was approximately 3 °C above ambient. This test was repeated three times for each cylinder to quantify the uncertainty. Once the *UA* value was found, the battery was heated and allowed to cool in a similar manner, with $\dot{q}_{\text{gen}} = 0$, to estimate the mC_p term for the battery. The uncertainty in the values is reported as the standard error shown in Eq. (5). A sample calibration run is shown in Fig. 6. The calibration results are shown in Table 2.

$$s_{\bar{x}} = \frac{\sigma_x}{\sqrt{n}} \tag{5}$$

3.3. Heat generation rates

The heat generated by the battery was found using Eq. (3) and the calibration values for constant power discharges at three different power levels as shown in Table 3.

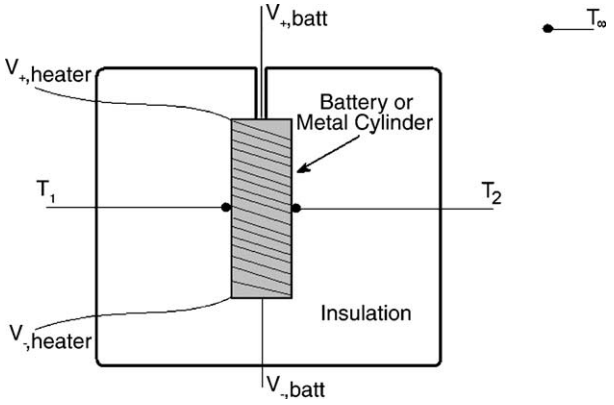

Fig. 5. Schematic of the experimental setup used to measure the battery heat generation rates.

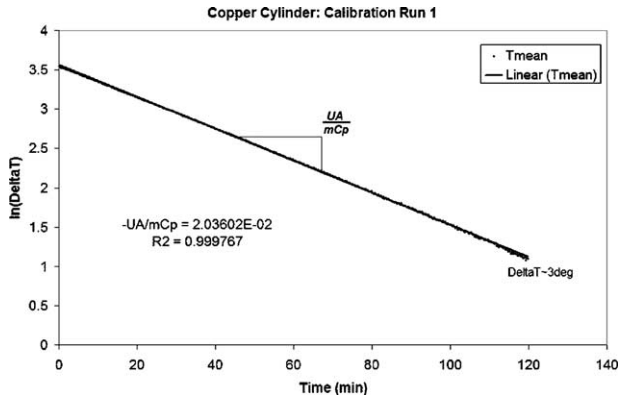

Fig. 6. Sample results of a calibration run with the copper cylinder.

Table 2
Calibration results valid from 60 to 3 °C above ambient temperature

Material	Mass (g)	Heat capacity (J g^{-1} K^{-1})	UA/mC_p (min^{-1})	Standard error (min^{-1})	UA (W K^{-1})	mC_p (J K^{-1})
Copper	149.1	0.385	−2.12E−02	±4.53E−4	1.91E−02 ± 1.63E−03	
Aluminium	44.5	0.896	−2.70E−02	±6.23E−4		
Li-ion battery	–	–	−2.91E−02	±5.66E−4	–	3.94E+01 ± 3.45E00

Table 3
Test conditions for heat generation tests

Battery power (W)	P-rate	Number of runs
6.6	P/1.25	5
4.125	P/2	5
2.75	P/3	5

Note: P-rate is analogous to the C-rate for a constant power discharge with a 8.25-Wh battery

Table 4
Standard error used to estimate the uncertainty in heat generation rates

Parameter	Standard error	Notes
mC_p (J K^{-1})	3.45	
dT (°C)	0.1	Approximate
dt (s)	0.01	Approximate
UA (W K^{-1})	0.00163	
ΔT (°C)	0.5	Approximate

Uncertainty in the calibration results and other parameters will propagate to the estimation of heat generation rate following Gaussian error propagation, shown for this case, in this case by Eq. (6).

$$s_{\bar{\dot{q}}\text{gen}} = \sqrt{(s_{\bar{\dot{q}}\text{stor}})^2 + (s_{\bar{\dot{q}}\text{conv}})^2}$$

$$\text{where } \left(\frac{s_{\bar{\dot{q}}\text{stor}}}{\dot{q}_{\text{stor}}}\right)^2 = \left(\frac{s_{\overline{mC_p}}}{mC_p}\right)^2 + \left(\frac{s_{\overline{\mathrm{d}T}}}{\mathrm{d}T}\right)^2 + \left(\frac{s_{\overline{\mathrm{d}t}}}{\mathrm{d}t}\right)^2$$

$$\left(\frac{s_{\bar{\dot{q}}\text{conv}}}{\dot{q}_{\text{conv}}}\right)^2 = \left(\frac{s_{\overline{UA}}}{UA}\right)^2 + \left(\frac{s_{\overline{\Delta T}}}{\Delta T}\right)^2 \quad (6)$$

The standard errors were either calculated from the calibration results, as shown in above, or were approximated by observing trends in the data. The values for the standard errors are shown in Table 4. In addition, the overall heat generation during a discharge cycle was approximated for each run by integrating the heat generation rate during the discharge.

4. Heat generation results

The voltage and current were measured for each discharge cycle. The mean voltage is shown in Fig. 7 along with the standard error in approximating the mean, from Eq. (5), for each DOD (depth of discharge) point. Similarly, the current data is shown in Fig. 8.

Since the batteries supply a constant power, the current produced by the battery increases as the voltage decreases. This is especially important at the end of the discharge cycle when the voltage quickly drops to the cut-off voltage of 3.0 V, causing the current to quickly increase. A brief examination

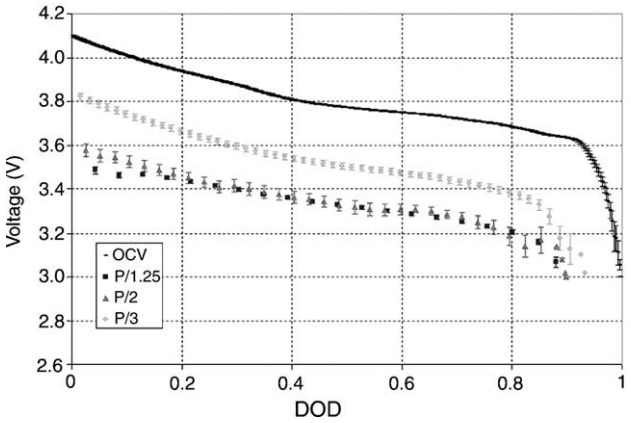

Fig. 7. Battery voltage during constant power discharge and OCV approximated with discharge at C/24 rate.

of Eq. (1) shows that the increasing current and decreasing voltage leads to an increase in the heat generation rate at the end of a constant power discharge.

The heat generation rate is shown for each cycle during constant power discharges in Fig. 9. A polynomial trend line was fit to each set of data to use in the simulations. The uncertainty in the heat generation rate was calculated for each point of each cycle; however, only the average uncertainty is reported for each discharge rate. For the most part, the uncertainty did not vary significantly throughout the discharge cycle.

Using the heat generation rates and the discharge characteristics of the battery, it is possible to estimate the en-

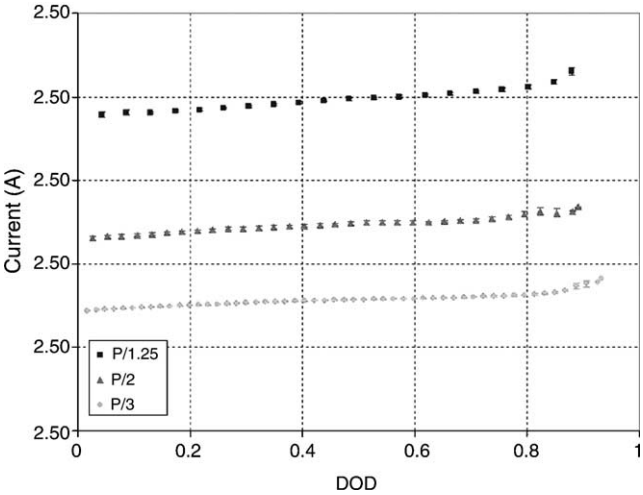

Fig. 8. Battery current during constant power discharge.

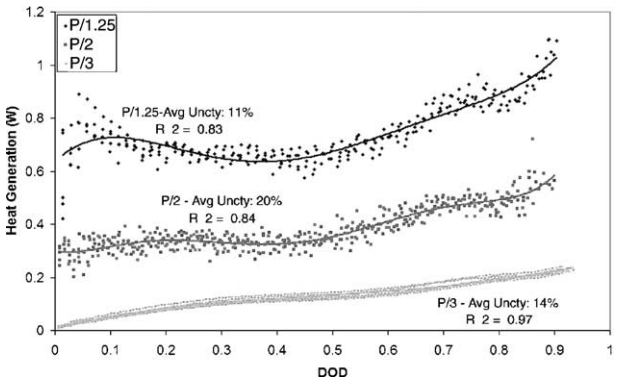

Fig. 9. Heat generation rate during constant power discharges.

tropy coefficient of the battery, used in Eq. (1), at each point of the discharge. Al-Hallaj et al. [10], modeled the entropy coefficient with a linear fit between two different discharge points. Similarly, a line was fit to the entropy coefficient data shown in Fig. 10 for the battery used in this study.

The thick, dark line represents the line fit to all of the points, for each discharge rate. The thin lines represent the line fit for all of the points during tests with similar discharge rates. As expected, the thin lines nearly collapse onto one trend line. However, the calculated entropy coefficient significantly diverges from the predicted trend near the end of the discharge for all three-power levels. Also, in theory the entropy coefficient should be independent of the discharge rate, which is not the case in the obtained results here. However, these findings and the magnitude of the measured values are consistent with trends in the entropy coefficient measured and reported in the literature [13].

The measured heat generation rate was compared to the heat generation rate that is predicted using the line fit to the entropy coefficient, shown in Fig. 11. In this chart, only one discharge cycle is used for each different power level, along with the uncertainty values calculated with Eq. (6).

Fig. 11 shows that the predicted heat generation rate during the *P*/3 discharge varies significantly from the rate measured

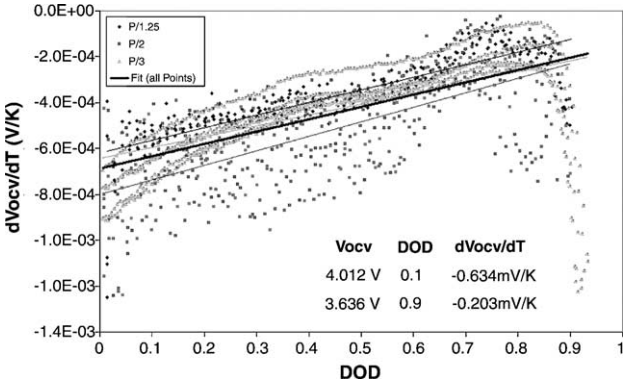

Fig. 10. Estimation of the entropy coefficient for the 2.2 Ah 18650 battery.

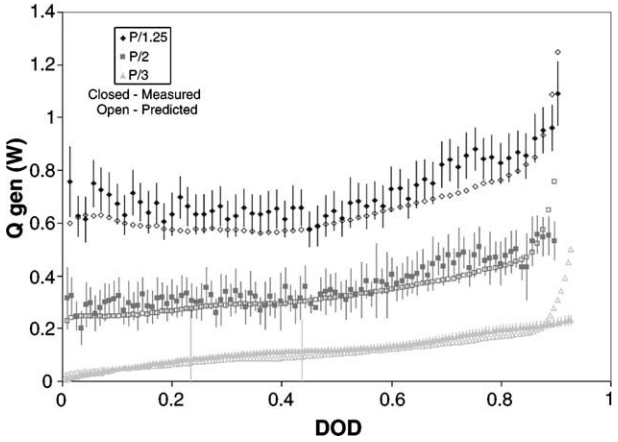

Fig. 11. Comparison of measured heat generation rate, Eq. (3), to rate predicted with entropy coefficient, Eq. (1).

Table 5
Total heat generation during constant power discharge

P-rate	Total heat generation (Wh)	
	Measured (%)	Predicted (%)
P/1.25	0.730 ± 0.66	0.676 ± 1.7
P/2	0.589 ± 0.93	0.626 ± 5.0
P/3	0.322 ± 0.73	0.309 ± 7.8

at the end of the discharge cycle. This may be an artifact of the measurement method (i.e. the thermal impedance of the Styrofoam washes out the sudden increase in heat generation at the end of the discharge) or simply due to the behavior of the battery.

Using both methods, the total heat generation was calculated for each discharge cycle. The mean values for the measured heat generation and the standard errors, again from Gaussian error propagation, are shown in Table 5 along with the predicted total heat generation using the entropy coefficient and the standard error calculated with Eq. (5).

Table 5 shows that increasing the discharge rate significantly increase the total heat generation. The use of the entropy coefficient estimated by the linear fit in Fig. 10 leads to slightly different heat generation rates, but still captures the general behavior of the batteries during discharge.

5. Performance simulations

A battery pack composed of six 2.2 Ah 18650 Li-ion batteries was simulated during a constant power discharge. The heat generation rate from the battery was the polynomial curve fit to the measured heat generation rates. The properties of the batteries and battery pack are shown in Table 6.

Table 6
Properties of the battery and battery pack used in simulations

Object	Thermal conductivity ($W\,m^{-1}\,K^{-1}$)	Heat capacity ($J\,g^{-1}\,K^{-1}$)	Density ($g\,m^{-3}$)
Battery	3	0.89	2.67E+06
Battery pack	0.2	1.8	1.21E+06
PCB	35 (y), 0.35 (x)	0.84	2E+06

5.1. Minimum volume simulation

First, the simulation was run for each power level for a complete discharge using a minimum volume (the depth of the pack is assumed to be the length of the batteries or 65 mm). The PCM/EG composite filled the gaps between the circular batteries and the rectangular battery pack, a total volume of $v_{avail} = 54.16\,cm^3$. The temperature distribution at the end of the P/1.25 discharge is shown in Fig. 12. Table 7 shows the maximum battery temperature during the discharge for the different heat generation rates, including the rates adjusted by the standard error from Table 5.

5.2. Battery pack design and simulation

As noted in the introduction, the temperature of the batteries should not exceed 55 °C during the battery discharge. Since the temperature of the batteries during the P/1.25 discharge exceeded 55 °C, the volume of the PCM/EG will need to be increased. Eq. (7) is true assuming all of the heat generated by the battery and electronics increases the latent and

Table 7
Maximum battery temperature during discharge for minimum volume battery pack with ambient temperature of 30 °C

Discharge rate	Total battery heat generation (Wh)	Maximum battery temperature (°C)
P/1.25	0.730 (Average)	64.76
P/1.25+	0.735 (Maximum)	65.01
P/1.25−	0.725 (Minimum)	64.52
P/2	0.589 (Average)	54.00
P/2+	0.594 (Maximum)	54.24
P/2−	0.584 (Minimum)	53.75
P/3	0.322 (Average)	45.66
P/3+	0.324 (Maximum)	45.72
P/3−	0.320 (Minimum)	45.61

Table 8
Volume needed for PCM/EG composite to keep temperature below 55 °C during constant power discharges with 30 °C ambient temperature

Case	Volume of PCM/EG, v_{comp} (cm^3)	Increase in volume (v_{comp}/v_{avail})
P/125	105.90	1.96
P/125 maximum	106.82	1.97
P/125 minimum	104.97	1.94
P/2	78.50	1.45
P/2 maximum	79.55	1.47
P/2 minimum	77.45	1.43
P/3	29.45	0.54
P/3 maximum	29.90	0.55
P/3 minimum	29.00	0.54

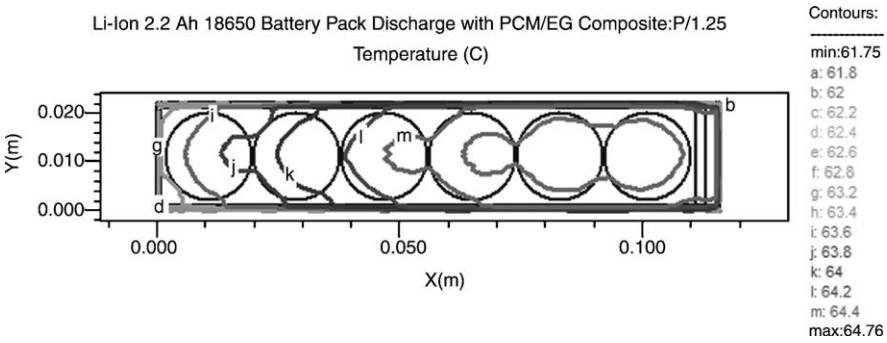

Fig. 12. Temperature contour of battery pack at end of P/1.25 discharge with minimum volume available for PCM/EG composite, ambient temperature is 30 °C.

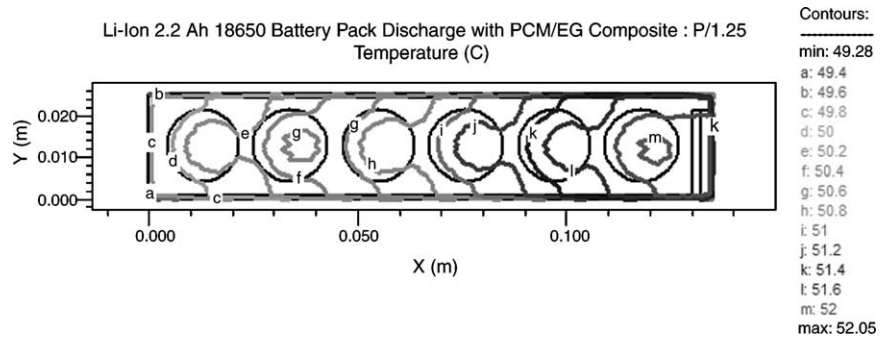

Fig. 13. Temperature contour for battery pack designed with $v_{comp} = 106.82\,cm^3$, P/1.25 discharge with 30 °C ambient temperature.

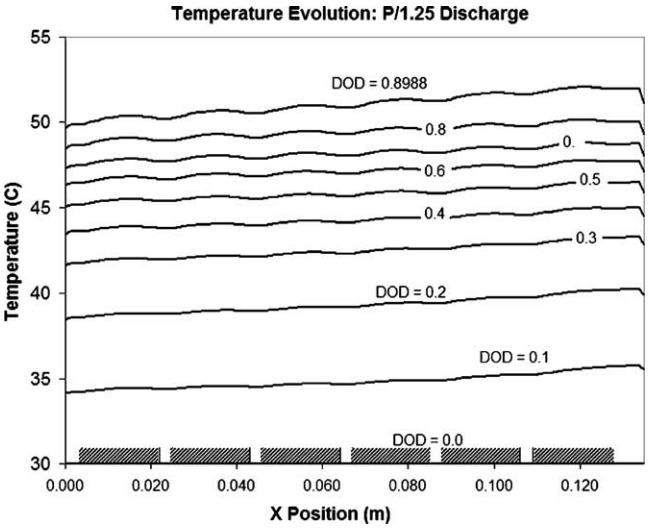

Fig. 14. Temperature evolution through center of battery pack (v_{comp} = 106.82 cm^3) during P/1.25 discharge with 30 °C ambient temperature; small rectangles represent positions of batteries.

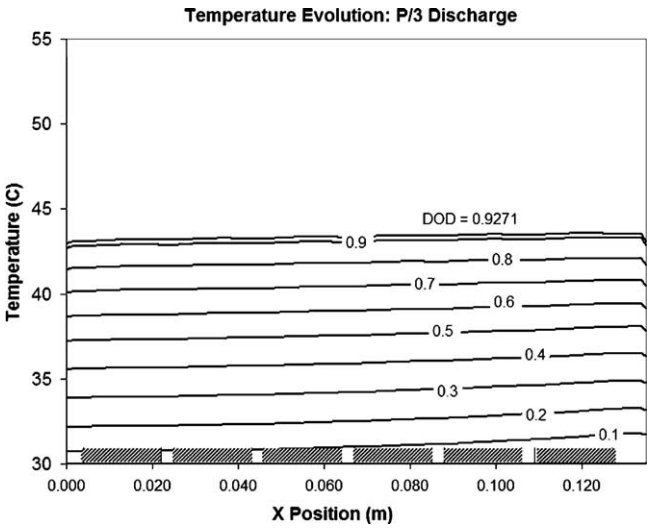

Fig. 16. Temperature evolution through center of battery pack (v_{comp} = 106.82 cm^3) during P/3 discharge with 30 °C ambient temperature.

sensible heat of the PCM/EG composite and the batteries, respectively. Solving Eq. (7) for the volume of the PCM/EG composite yields a conservative estimate of the volume necessary to keep the batteries below the maximum temperature of 55 °C while operating in an environment at 30 °C.

$$\dot{q}_{gen} + \dot{q}_{elect} = \dot{q}_{sensible} + \dot{q}_{latent} \quad (7)$$

Table 8 shows the volume of composite, V_{comp} calculated from Eq. (7), for each discharge power as well as the ratio of the necessary volume of PCM/EG to the available volume. Picking the P/1.25 maximum case for the volume target (v_{comp} = 106.82 cm^3), a battery pack was designed to meet the design criteria. Fig. 13 shows the temperature contours for the P/1.25 case. Figs. 14–16 show the evolution of the temperature profile for different discharge powers with the expanded battery pack.

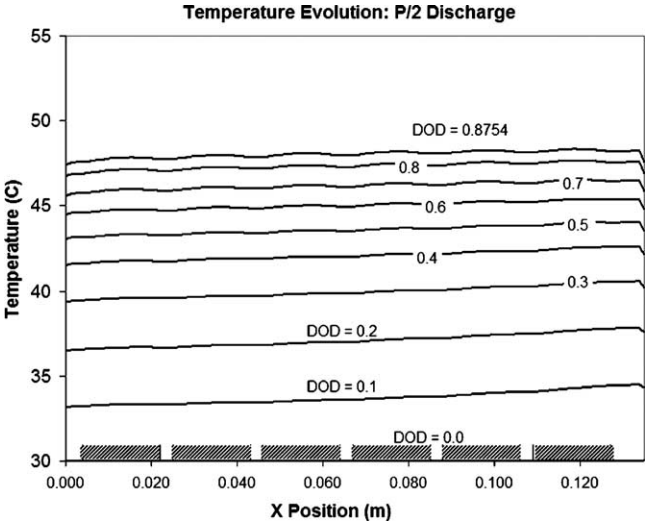

Fig. 15. Temperature evolution through center of battery pack (v_{comp} = 106.82 cm^3) during P/2 discharge with 30 °C ambient temperature.

Table 9
Ideal properties of the PCM/EG plausible with advanced manufacturing techniques

Property	Value
Thermal conductivity (W m^{-1} K^{-1})	25
Latent heat (J g^{-1})	180
Specific heat (J g^{-1} K^{-1})	2.25
Bulk density of composite (g m^{-3})	1.01E+06
Bulk density of graphite (g m^{-3})	2.1E+05

5.3. Ideal composite

The performance of the battery pack was simulated for a composite with improved properties. These improvements may be possible with advanced techniques for fabrication of the PCM/EG composites. Table 9 shows the characteristics of the PCM/EG used in this section. The results of the simulation show that a battery pack made with the improved properties will only need v_{comp} = 59.53 cm^3 to maintain a temperature below 55 °C during the highest discharge. The volume of the ideal composite is only 9.9% more volume than is available in the gaps around the batteries in the unmodified battery pack described above.

6. Conclusions

The simple heat generation measurement method outlined in this work produced the heat generation rates for 186502.2 Ah batteries during constant power discharges with high precision. The detailed discharge profiles showed that the measured heat generation rate and heat generation rate

predicted using the entropy coefficient method leads to similar results.

Simulation results showed that although the total heat generation from the battery is only a fraction of the electrical energy produced by the battery, battery temperatures could quickly rise to levels that will adversely affect the lifetime of the batteries and become a safety issue. Increasing the volume of the battery pack and amount of PCM, about doubling it in this case, significantly improved the performance of the thermal management system; meeting the criteria of an operating temperature lower than 55°C even at the high discharge rate. The conservative estimate in the volume needed to meet the temperature criteria ensures that the criteria will be met even if the ambient temperature slightly increases.

The final simulation using the PCM/EG composite with ideal properties shows that the passive thermal management system utilizing advanced manufacturing techniques can minimize temperature swings during high power discharges with only a 10% increase in battery pack volume.

Acknowledgments

The authors thank Shabab Amiruddin for his technical assistance and the MMAE Machine Shop Technicians for fabrication of samples. The authors also acknowledge All Cell Technologies, LLC (Chicago, IL) for providing scholarship funds for Andrew Mills. Technical support by MicroSun Technologies, LLC (Lisle, IL) is acknowledged.

References

[1] P. Ramadass, B. Haran, R. White, B.N. Popov, J. Power Sources 112 (2002) 614–620.
[2] H. Maleki, A. Shamsuri, Thermal analysis and modeling of a notebook computer battery, J. Power Sources 115 (2003) 131–136.
[3] S.A. Khateeb, M.M. Farid, J.R. Selman, S. Al-Hallaj, J. Power Sources 128 (2004) 292–307.
[4] M.M. Farid, A.M. Kuhdair, S.A. Khateeb, S. Al-Hallaj, A review on phase change energy storage: materials and applications, Energy Convers. Manage. 45 (2004) 1597–1615.
[5] A. Mills, M. M. Farid, S. Al-Hallaj, Thermal conductivity enhancement of phase change material using a graphite matrix, J. Appl. Therm. Eng., submitted for publication.
[6] X. Py, R. Olives, S. Mauran, Paraffin/porous-graphite–matrix composite as a high and constant power thermal storage material, Int. J. Heat Mass Transfer 44 (2001) 2727–2737.
[7] J. Han, K. Cho, K. Lee, H. Kim, Porous graphite matrix for chemical heat pumps, Carbon 36 (1998) 1801–1810.
[8] M. Bonnissel, L. Lou, D. Tondeur, Compacted exfoliated natural graphite as a heat conduction medium, Carbon 39 (2001) 2151–2161.
[9] M. Farid, F. Hamad, M. Abu-Arabi, Melting and solidification in multi-dimensional geometry and presence of more than one interface, Energy Convers. Manage. 39 (1998) 809–818.
[10] S. Al Hallaj, H. Maleki, J. Hong, J. Selman, Thermal modeling and design considerations of lithium-ion batteries, J. Power Sources 83 (1999) 1–8.
[11] J.P. Holloman, Heat Transfer, 5th ed., McGraw-Hill Book Co., New York, 1981, pp. 285–288.
[12] H. Maleki, A. Al-Hallaj, J.R. Selman, R.B. Dinwiddle, H. Wang, Thermal properties of lithium-ion battery and components, J. Electrochem. Soc. 146 (1999) 947–954.
[13] S. Al Hallaj, J.R. Selman, Entropy changes due to structural transformation in the graphite anode and phase change of the $LiCoO_2$ cathode, J. Electrochem. Soc. 147 (9) (2000) 3231–3236.